Impurity effect on the melting of nickel clusters as seen via molecular dynamics simulations

Andrey Lyalin,[1,2,3,*] Adilah Hussien,[1] Andrey V. Solov'yov,[1,†] and Walter Greiner[1]
[1]*Frankfurt Institute for Advanced Studies, Goethe-University, Ruth-Moufang-Strasse 1, 60438 Frankfurt am Main, Germany*
[2]*Department of Physics, Imperial College London, Prince Consort Road, London SW7 2BW, United Kingdom*
[3]*Division of Chemistry, Graduate School of Science, Hokkaido University, Sapporo 060-0810, Japan*
(Received 8 August 2008; revised manuscript received 9 February 2009; published 6 April 2009)

We demonstrate that the addition of a carbon impurity leads to significant changes in the thermodynamic properties of a Ni_{147} cluster. The magnitude of the change induced is dependent on the parameters of the Ni-C interaction. Hence, thermodynamic properties of Ni clusters can be effectively tuned by the addition of a particular type of impurity. We also show that the presence of a carbon impurity considerably changes the mobility and diffusion of atoms in the Ni cluster at temperatures close to its melting point. The calculated diffusion coefficients of the carbon impurity in the Ni cluster can be used as a reliable estimate of the growth rate of carbon nanotubes.

DOI: 10.1103/PhysRevB.79.165403 PACS number(s): 65.80.+n, 64.60.an

I. INTRODUCTION

Thermodynamic properties of atomic clusters depend significantly on the size of the cluster. It has been shown that the melting temperature of a small spherical particle decreases with the reduction in its radius.[1–5] This is due to the substantial increase in the relative number of weakly bounded atoms on the surface in comparison with those in the bulk. Such a size effect on the melting temperature of small metal clusters having diameters down to 2–3 nm has been confirmed in a series of experiments.[6–9]

However for clusters having sizes smaller than 1–2 nm, the melting temperature is no longer a monotonic function of the cluster size. Experiments on sodium clusters Na_N, with number of atoms $N=50-360$, have demonstrated that melting temperature as a function of size shows a prominent irregular structure with the local maxima.[10–13] The origin of the nonmonotonic variation in the melting temperature with respect to cluster size lies in the interplay between electronic and geometric shell effects in the sodium clusters.[13] Intensive theoretical efforts have been undertaken to identify the details of the geometric and electronic structures underlying the variations in the melting temperature.[14–21]

Experiments on small ion clusters of tin[22] and gallium[23] have confirmed the violation of the linear relationship between the reduction in the melting temperature and the inverse radius of the cluster. It was discovered that the melting temperature of selected Sn_N and Ga_N clusters, of sizes $N<40$, can considerably exceed the melting temperature of the corresponding bulk material.[22,23] This behavior was explained by the structural differences between the small clusters and the bulk.[22]

Modification of a cluster structure can also be induced by the doping of an impurity or substitution of one or several atoms in a pure cluster with an atom of a different type.[24] It has been shown that doping of sodium clusters with Li, Cs, and O_2 impurities (as well as Al_{13} and Ga_{13} clusters with a carbon impurity) results in a decrease in the melting temperature of the cluster.[25–27] Whereas doping of the icosahedral silver clusters with Ni and Cu atoms considerably increases the melting temperature.[28] Therefore one can suppose that the thermodynamic properties of a selected cluster can be tuned by doping with an impurity of a particular type. Thus, it was demonstrated in Ref. 29 that alloying iron clusters consisting up to 2400 atoms with carbon reduce its melting temperature by 100–150 K at a carbon concentration of 10%–12%. Recently the thermal behavior of free and alumina-supported Fe-C nanoparticles has been investigated.[30] It was observed that the presence of the substrate raises the melting temperature of medium and large $Fe_{(1-x)N}C_{xN}$ nanoparticles ($x=0-0.16$, $N=80-1000$) by 40–60 K.[30]

In this paper we report the results of a systematic theoretical study regarding the effect of impurity on the thermodynamic properties of Ni clusters. We demonstrate that adding a single carbon impurity can result in changes in the melting temperature of an Ni_{147} cluster. The magnitude of the change induced is dependent on the parameters of the interaction between the Ni atoms and the C impurity. Hence, thermodynamic properties of Ni clusters can be effectively tuned by the addition of an impurity. We also show that the presence of a carbon impurity considerably changes the mobility of atoms in the Ni cluster at temperatures close to its melting point.

The choice of Ni clusters is stipulated by their high chemical and catalytic reactivity, unique properties, and multiple applications in nanostructured materials.[31] An important example of such an application is the process of the catalytically activated growth of carbon nanotubes. The mechanism of this process is not yet well understood (see, e.g., Refs. 29 and 32–39 and references therein) and knowledge of the specific role of the impurity in the Ni catalytic nanoparticle may ascertain whether the carbon nanotube structure and its growth kinetics can be controlled. The thermodynamic state of the catalytic nanoparticle plays a crucial role on the carbon nanotube growth.[40] The important question is whether the catalytic nanoparticle is molten or frozen during the nanotube growth process. It was demonstrated that when carbon nanotubes are grown on large (>3–4 nm) iron nanoparticles at temperatures lower than 1200 K, the catalytic particle is not completely molten.[29] Thus, the mechanism of nanotube growth can be governed by the surface melting of the cluster.[29] On the other hand, it was demonstrated that the

reduction in the catalyst size requires an increase in the minimum temperature necessary for the growth of the single-walled carbon nanotubes due to the reduction in a carbon solubility in the metal nanoparticle.[38] The nanotube growth rate can be obtained by a solution of a set of kinetic equations which include, in particular, the diffusion flux of carbon through the metal particle.[34,41,42] On the other hand the diffusion coefficients depend on the thermodynamic state of the catalytic Ni cluster which can, in turn, be tuned by doping with an impurity. Therefore direct molecular dynamics studies of carbon diffusion in the Ni cluster are important for a reliable estimation of the growth rate of carbon nanotubes.

II. THEORETICAL METHODS

The study of structural and dynamical properties of transition-metal clusters is a challenging task due to the presence of unfilled valence *d* orbitals. The high density of the *d* states and their localized character make the direct *ab initio* methods computationally very demanding for clusters larger than several dozens of atoms.[43] In order to describe the structure of clusters of larger sizes, one needs to use approximate methods and model interatomic potentials.

An effective approach for study of transition-metal clusters is the embedded-atom method[44–49] which takes into account many-body effects. The latter appears through the inhomogeneous electron density of the system. In this paper, the molecular dynamics study of the Ni_{147} cluster has been performed using the Sutton-Chen[44] many-body potential which belongs to the family of the embedded-atom types of potentials. The Sutton-Chen potential[44] has been shown to reproduce bulk and surface properties of transition metals and their alloys with sufficient accuracy (see, e.g., Refs. 43 and 50–53 and references therein). The applicability of the Sutton-Chen potential[44] to Ni clusters has been proven by the direct comparison of the optimized structures and the binding energies of small Ni clusters obtained within the *ab initio* method and with the use of the Sutton-Chen potential.[43,44] The potential energy of the finite system within the Sutton-Chen model[44] has the following form:

$$U_{\mathrm{pot}} = \varepsilon \sum_i \left[\frac{1}{2} \sum_{j \neq i} \left(\frac{a}{r_{ij}} \right)^n - c \rho_i^{1/2} \right], \tag{1}$$

where

$$\rho_i = \sum_{j \neq i} \left(\frac{a}{r_{ij}} \right)^m. \tag{2}$$

Here r_{ij} is the distance between atoms i and j, ε is a parameter with dimension of energy, a is the lattice constant, c is a dimensionless parameter, and n and m are positive integers with $n > m$. The parameters provided by Sutton and Chen[44] for nickel have the following values: $\varepsilon = 1.5707 \times 10^{-2}$ eV, $a = 3.52$ Å, $c = 39.432$, $n = 9$, and $m = 6$.

The determination of a reliable model potential for the Ni-C interaction is a difficult task. In Refs. 54–56, the binding energy and different charge state of various forms of NiC_n clusters ($n = 1-3$) were determined using *ab initio* density functional calculations based on the three-parameter Becke-type gradient-corrected exchange functional with the gradient-corrected correlation functional of Lee *et al.*[57] (B3LYP) (Refs. 58 and 59) and LANL2DZ basis set (see, e.g., Ref. 60 and references therein). This was done in order to develop a many-body potential for the transition-metal-carbon interaction. The many-body potential was then successfully used for a molecular dynamics study of the formation of metallofullerenes[54] and single-walled carbon nanotubes.[55]

In the present work, however, the interaction between Ni atoms and C impurity is modeled by the Morse pair potential,

$$V^{\mathrm{Ni\text{-}C}}(r) = \varepsilon_M [(1 - e^{\rho(1 - r/r_0)})^2 - 1]. \tag{3}$$

We have determined the parameters of the Morse potential ($\varepsilon_M = 2.431$ eV, $\rho = 3.295$, and $r_0 = 1.763$ Å) by fitting the Ni-C interaction obtained in Refs. 54–56 within the B3LYP/LANL2DZ method. The choice of using the pairwise Morse potential is due to its simplicity which allows us to study the influence of the parameters in Eq. (3) on the thermodynamic properties of the C-doped Ni_{147} clusters, keeping a clear physical picture of the process occurring in the system.

The covalent bonding between the carbon atoms inside Ni_{147} cluster is modeled by the Tersoff potential.[61] We should note, however, that the Tersoff potential[61] may overestimate the C-C bonding inside the host cluster. It is a difficult task to find a reliable many-body potential for the C-C interactions inside the metal cluster. The parameters of such a potential should be based on the *ab initio* quantum mechanical calculations for the considered compound system. Currently the systematic *ab initio* study of interatomic interactions in the mixed Ni_nC_m systems is performed only for small clusters.[62,63]

The optimized initial geometries of the cluster have been determined by finding local minima on the multidimensional potential energy surface. We have applied an efficient scheme of global optimization, called the cluster fusion algorithm (CFA).[64–66] The CFA belongs to the class of genetic global optimization methods,[67,68] which are very promising for structural optimization of nanoalloys (see, e.g., Ref. 69 and references therein). The scheme has been designed within the context of determining the most stable cluster geometries and is applicable for various types of clusters.[64,70–72]

Molecular dynamics simulations have been performed for the canonical (*NVT*) ensemble of particles: the number of particles N, the volume V, and the temperature T of the system are kept constant. Integration of Newton's equations of motion has been done using the Verlet leap frog algorithm, with a time step $\Delta t = 1$ fs and a total simulation run of 10 ns (excluding an initial equilibration time of 50 ps). For temperature control, we have used the Nose-Hoover thermostat[73,74] because it correctly generates a canonical ensemble.

III. NUMERICAL RESULTS AND DISCUSSION

During the last decade, numerous theoretical and experimental efforts have been devoted for studying structural,

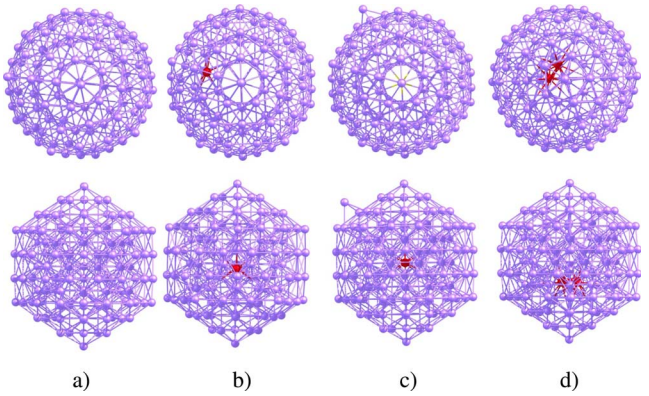

FIG. 1. (Color online) (a) Optimized structure of a pure Ni_{147} cluster; (b) the *isomer* state structure of the C-doped Ni_{147} cluster; (c) the *ground* state structure of the C-doped Ni_{147} cluster; and (d) the optimized structure of the C_2-doped Ni_{147} cluster.

electronic, and magnetic properties of Ni clusters (recent comprehensive reviews can be found in Refs. 75 and 76). It has been demonstrated that for small Ni clusters, a motif based on the icosahedral structure dominates the cluster growth, at least around sizes of the complete Mackay icosahedra.[53,77–79] The results of the geometry optimization for the pure and the C-doped Ni_{147} clusters are shown in Fig. 1. The ground state of the Ni_{147} cluster is a perfect icosahedron [Fig. 1(a)], in agreement with the results of the previous works (see Refs. 75 and 79 and references therein).

For the C-doped Ni_{147} cluster, we have found that the lowest energy state possesses an icosahedral type of structure with the C atom in the central position and one Ni atom outside the filled icosahedral shell, as shown in Fig. 1(c). The energetically closest isomer of the C-doped Ni_{147} cluster is the deformed icosahedron with the C impurity located in the vicinity of the cluster center, as depicted in Fig. 1(b). The impurity creates a local distortion between the first and the second closed icosahedral shells. The difference in the binding energy per atom between the ground [Fig. 1(c)] and the isomer [Fig. 1(b)] states of the C-doped Ni_{147} cluster is 0.002 eV. The isomer state [Fig. 1(b)] is metastable because in order to transform the cluster structure from the isomer [Fig. 1(b)] to its ground state [Fig. 1(c)], it is necessary to overcome the energy barrier. The isomer [Fig. 1(b)] can be naturally formed by successive migration of the outer C atom from the cluster surface toward its center. Namely, this type of isomer is presumably formed in carbon nanotube growth experiments where a molecule of a feedstock gas or a free C atom collides with the surface of the Ni particle. Therefore, we have performed molecular dynamics simulations for the initial geometry corresponding to the isomer state [Fig. 1(b)] of the C-doped Ni_{147} cluster. The optimized structure of the C_2-doped Ni_{147} cluster is shown in Fig. 1(d).

A. Pure Ni_{147} clusters

Figures 2 and 3 demonstrate the temperature dependence of the time-averaged total energy $\langle E_{\mathrm{tot}} \rangle$ (i.e., the caloric curve) and the heat capacity C_V calculated for the Ni_{147} cluster, respectively. The heat capacity at constant volume is defined as a derivative of the internal energy over the temperature: $C_V = (\partial E / \partial T)_V$.

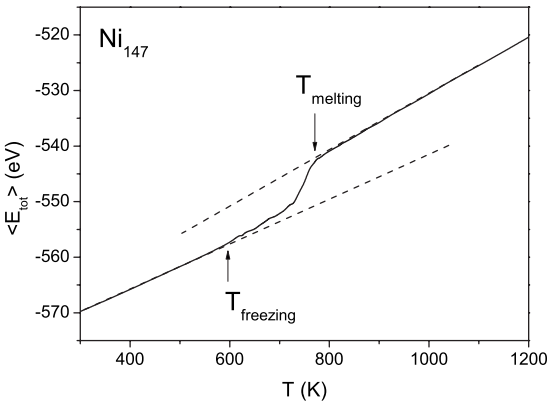

FIG. 2. Caloric curve for the pure Ni_{147} cluster. Temperatures $T < T_{\mathrm{freezing}}$ and $T > T_{\mathrm{melting}}$ correspond to the completely frozen and melted states, respectively. (Dashed lines) Extrapolation of the frozen and molten branches of the caloric curve to estimate the latent heat. The total simulation time is 10 ns.

A thermal phase transition is indicated in the caloric curve by a change in the gradient of the temperature-dependent total energy $\langle E_{\mathrm{tot}} \rangle$. The height of the jump near the phase transition point gives an estimate of the latent heat, i.e., the energy which is associated with the destruction of the ordered lattice. Figure 2 demonstrates that the change in the slope of the caloric curve takes place in the wide interval of temperatures between $T_{\mathrm{freezing}} \approx 600$ K and $T_{\mathrm{melting}} \approx 800$ K. For the temperatures $T < T_{\mathrm{freezing}}$, the cluster is completely frozen, while for temperatures $T > T_{\mathrm{melting}}$, the cluster has melted. Temperatures $T < T_{\mathrm{freezing}}$ and $T > T_{\mathrm{melting}}$ are stable with the time of simulation only for the long enough run of 10 ns or more, which was confirmed by the control simulations of 50 ns. The intermediate interval $T_{\mathrm{freezing}} < T < T_{\mathrm{melting}}$ corresponds to the mixed state where the solid and the liquid phases coexist. This is a typical behavior of the caloric curve for finite systems, in contrast to the abrupt stepwise jump of the caloric curve corresponding to the melting temperature of a bulk.

The melting process can also be easily recognized by the peak in the temperature dependence of the heat capacity, as

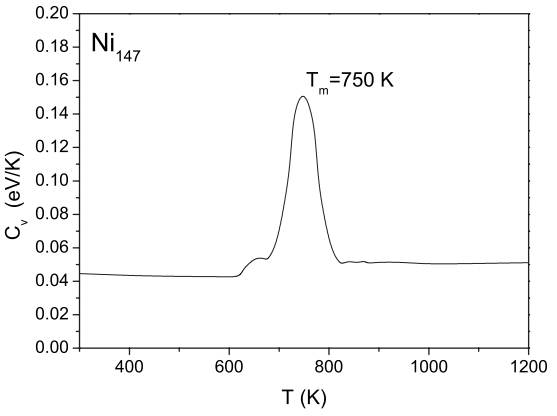

FIG. 3. Heat capacity for the pure Ni_{147} cluster as a function of T. Temperature $T_m = 750$ K indicates the melting temperature of the cluster (defined as the maximum of the heat capacity).

seen in Fig. 3. We have found that for the pure Ni_{147} cluster, the melting temperature associated with the maximum of the heat capacity T_m=750 K is considerably smaller than the melting temperature for the bulk nickel T_m^{bulk}=1728 K.[80] As was discussed above, the decrease in the melting temperature of the finite size clusters in comparison with the bulk occurs due to a substantial increase in the relative number of weakly bounded atoms on the cluster surface. According to the so-called "Pawlow law"[2] the melting temperature of a spherical particle possessing a homogeneous surface decreases linearly with increasing its inverse radius,

$$T_m = T_m^{\text{bulk}}\left(1 - \frac{\alpha}{R}\right), \tag{4}$$

where R is the radius of the spherical particle and α is a constant, which can be defined by fitting the temperature T_m to available experimental data. Equation (4) is valid for the relatively large particles when shell effects are not important. The similar reduction in the melting temperature of the large Ni_N clusters with the number of atoms N ranging from 336 to 8007 has been reported in Ref. 5. Thus, it has been shown that the melting temperature calculated with the use of a Sutton-Chen-type force field drops[44] from 1760 K (calculated melting temperature of bulk nickel) to 980 K for the Ni_{336} cluster.[5] Note that the theoretical prediction of the melting temperature of bulk nickel (1760 K) is in good agreement with the experimental data (1728 K). Based on the calculated melting temperatures from Ref. 5, we have estimated the values of T_m^{bulk} and α in Eq. (4) to be 1590 K and 3.65 Å, respectively. The radius of the cluster has been defined as $R=r_sN^{1/3}$, where r_s=1.375 Å is the Wigner-Seitz radius for bulk nickel.[81] The difference of the estimated value of T_m^{bulk} in Eq. (4) and the calculated melting temperature of bulk nickel partly occurs due to the fact that the finite cluster calculations have a free surface, whereas the bulk calculations do not.[5] Similar dependence of the melting temperature as a function of cluster size was reported in Ref. 29 for the pure iron and alloyed iron-carbide clusters.

Apart from the main peak, the heat capacity displays an additional maximum at $T \approx 660$ K—suggesting a stepwise melting process. This additional maximum corresponds to a slight change in the slope of the caloric curve beginning at $T_{\text{freezing}} \approx 600$ K. Such a situation corresponds to the so-called *premelted* state—when the cluster surface melts first while the core of the cluster remains frozen. This is the stationary state where the coexistence of two phases—liquid surface and frozen cluster core—is observed. The exact delimitation of the two phases is relative but can be defined from the difference in the mobility of atoms taken from the cluster surface and its core. Visualization of the molecular dynamics trajectories of atoms located at the surface and in the core of the cluster as well as analysis of the time-averaged atomic radial distribution in the cluster confirms this interpretation (see Figs. 11 and 12 and the following discussion). The premelting effect has also been observed in Ref. 5 for large Ni clusters. In general, the appearance of the premelted state depends on the parameters of interatomic interaction in a finite size cluster. In Ref. 82 the influence of the softness of the repulsive core interaction on the melting of 13-particle clusters has been studied for the family of pairwise additive inverse-power-based potentials. A two-step melting was observed for soft-core repulsion potentials, while for harder potentials, the two steps were merged into one.[82] A systematic analysis of the melting transition in the selected Na, K, Rb, and Cs clusters has been performed in Refs. 20 and 83–85. It was demonstrated that a surface melting stage develops upon heating before homogeneous melting temperature is reached. In the series Na→K→Rb→Cs, the premelting effects are more important for the heavier elements.[84] Since the repulsive part of the pseudopotentials used in Ref. 84 is harder for the lighter alkali element, the importance of premelting effects increases with the series Na→K→Rb→Cs.

Figures 4(a)–4(c) present the time dependence of the instantaneous values of the total energy (i.e., the total energy of the system, E_{tot}, at the moment of time t) calculated for the Ni_{147} cluster at the temperatures of 600, 750, and 800 K, respectively. The total simulation time is 10 ns.

It is seen from Fig. 4(a) that the instantaneous values of the total energy, E_{tot}, oscillate around their time-averaged value $\langle E_{\text{tot}} \rangle$ at the cluster temperature T=600 K. The fluctuation in the instantaneous total energy of the system is a result of choosing the canonical ensemble of particles. To reproduce this ensemble, the temperature of the system is controlled by the Nose-Hoover thermostat,[73,74] which produces the appropriate energy fluctuations. The frozen phase is characterized by thermal vibrations of the atoms around equilibrium positions in the cluster lattice, while the overall cluster structure remains unchanged.

For the temperature T=750 K, corresponding to the maximum of the heat capacity, the time dependence of the instantaneous values of the total energy changes, as shown in Fig. 4(b). The total energy of the system, E_{tot}, initially oscillates around its typical averaged value for the frozen Ni_{147} state. After some time, the system jumps to a disordered molten state—causing the total energy of the system E_{tot} to oscillate around the average value typical for the molten Ni_{147} state. The system then, after a finite period in the molten state, jumps back to its initial frozen state. This behavior is repetitive and the system continuously oscillates between the frozen and molten states. The time development of the time-averaged total energy $\langle E_{\text{tot}} \rangle$ of the Ni_{147} cluster at the phase transition point is demonstrated by the dashed-dotted line in Fig. 4(b). It is seen from Fig. 4(b) that averaged total energy $\langle E_{\text{tot}} \rangle$ becomes time independent after a simulation time of 6 ns or more. Thus, in the interval of temperatures $T_{\text{freezing}} < T < T_{\text{melting}}$, it is necessary to perform the molecular dynamics simulations for a relatively long time (on the order of 10 ns) to achieve time independence of the averaged total energy $\langle E_{\text{tot}} \rangle$ of the system. Such long simulation times are difficult to achieve by *ab initio* molecular dynamics methods.

The average lifetime of the system in the frozen and the molten states depends on the temperature of the cluster, resulting in a smooth change in the $\langle E_{\text{tot}} \rangle$ from the frozen to the molten state as a function of temperature. Thus, Fig. 4(b) clearly demonstrates the coexistence of both thermodynamic phases of the finite system at the temperature of phase transition. A similar behavior of the time dependence of the

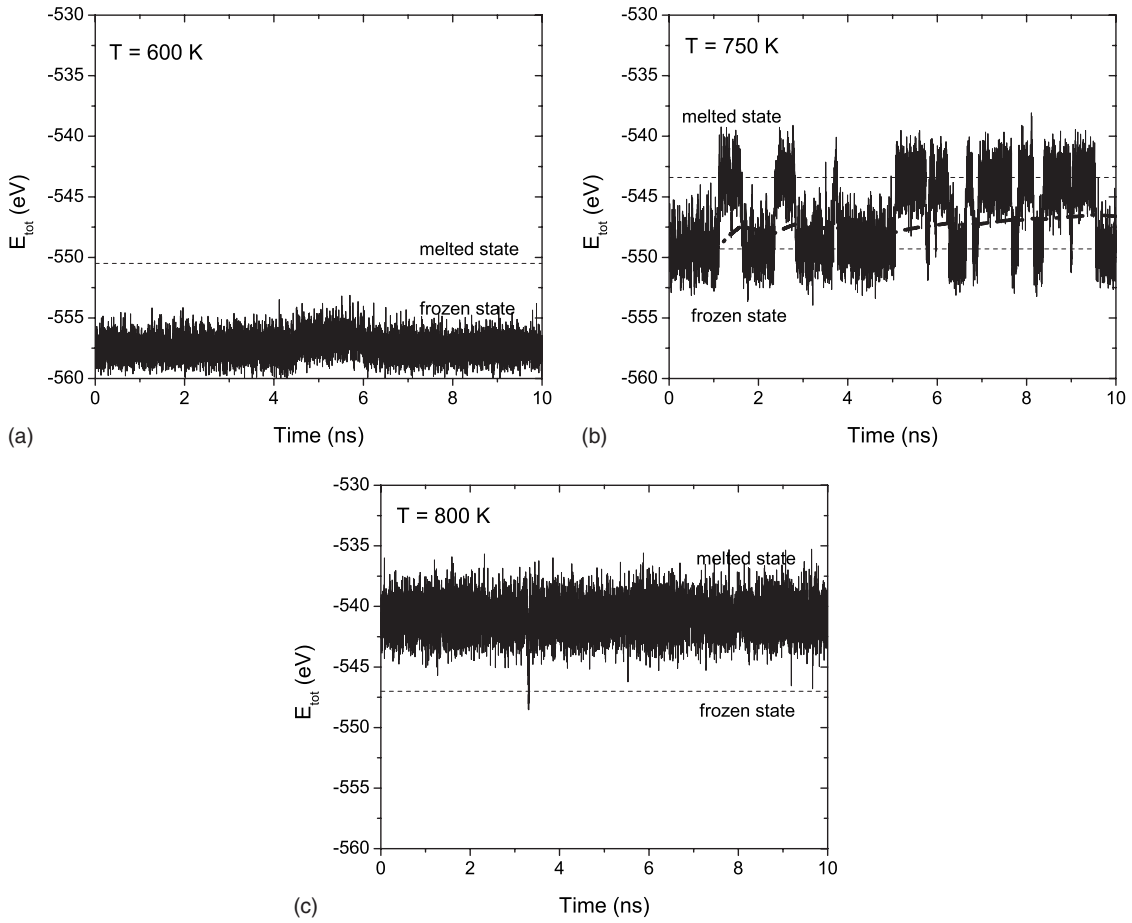

FIG. 4. Time dependence of the instantaneous values of the total energy calculated for the Ni_{147} cluster: (a) $T=600$ K, frozen state; (b) $T=750$ K, phase transition; and (c) $T=800$ K, molten state. The dashed-dotted line demonstrates the time development of the time-averaged total energy of the system at the point of phase transition. The dashed lines correspond to the long time-averaged total energy of the system estimated from the frozen and molten branches of the caloric curve.

short-time potential energy averages calculated for the Ar_{13} cluster at the temperature of 33 K has been reported in Refs. 86 and 87. Finally, for the temperature $T=800$ K and above, the instantaneous total energy of the Ni_{147} cluster oscillates around its typical averaged value for the molten state.

B. Carbon-doped Ni_{147} clusters

We now focus our study on the thermodynamic properties of the carbon-doped Ni_{147} clusters. We consider a cluster with the C and C_2 impurities in the vicinity of the cluster center as shown in Figs. 1(b) and 1(d), respectively.

Dashed-dotted and dotted lines in Figs. 5 and 6 demonstrate the temperature dependence of the caloric curve and the heat capacity calculated for the C-doped Ni_{147} and the C_2-doped Ni_{147} clusters, respectively. For the sake of comparison, we have plotted the same dependencies calculated for the pure Ni_{147} cluster in Figs. 5 and 6 by solid lines. As seen in Figs. 5 and 6, doping of the Ni_{147} cluster with a single C impurity reduces its melting temperature by 30 K. Thus, doping of a cluster consisting of more than a hundred of atoms by just one additional atom of impurity results in a considerable change in its melting temperature.

Figure 5 demonstrates that the first change in the slope of the temperature-dependent $\langle E_{tot}\rangle$ calculated for the C-doped Ni_{147} cluster occurs at a temperature slightly below 600 K. This indicates that the C impurity does not have much influ-

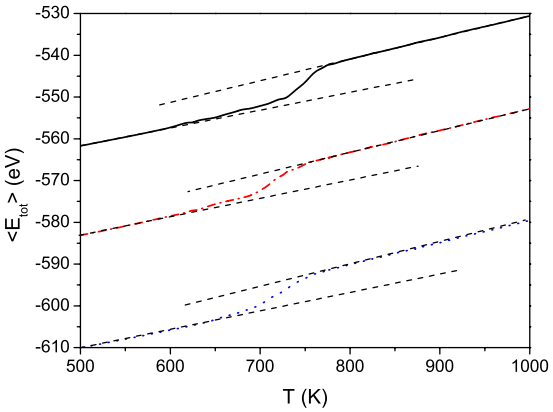

FIG. 5. (Color online) Caloric curve for the pure Ni_{147} cluster (solid line), the C-doped Ni_{147} cluster (dashed-dotted line), and the C_2-doped Ni_{147} cluster (dotted line). (Dashed lines) Extrapolation of the frozen and molten branches of the caloric curve to estimate the latent heat. The total simulation time is 10 ns.

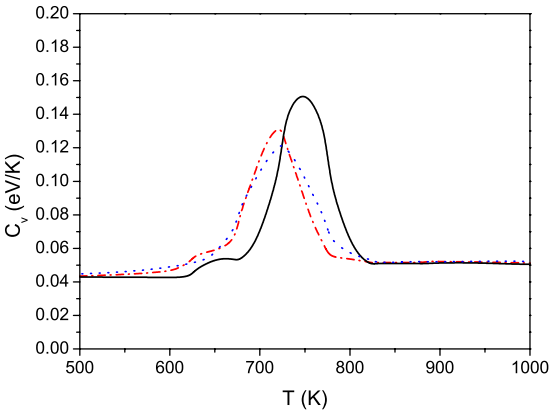

FIG. 6. (Color online) Heat capacity for the pure Ni_{147} cluster (solid line), the C-doped Ni_{147} cluster (dashed-dotted line), and the C_2-doped Ni_{147} cluster (dotted line) as a function of T. Temperatures T_m=750, 720, and 725 K corresponds to the melting temperatures of the pure, the C-doped Ni_{147}, and the C_2-doped Ni_{147} cluster, respectively.

ence on the surface melting of the cluster. Indeed, the C impurity is located near the cluster center where it induces local deformations. However, it does not significantly change the structure of the cluster surface [see Fig. 1(b)]; therefore, it does not have much of an effect on surface melting.

Further increase in the cluster temperature results in the melting of the C-doped Ni_{147} cluster with the melting temperature T_m=720 K. The latter is defined by the position of the maximum of the temperature-dependent heat capacity. The decrease in the melting temperature of the C-doped Ni_{147} cluster can be explained as a result of the distortion of the cluster's icosahedral structure. The C atom introduces deformation in the cluster lattice which decreases the stability of the cluster thus, its melting temperature. Similar considerations can be applied to the Ni_{147} cluster doped with a C_2 molecule. Analysis of the molecular dynamics trajectories shows that the C_2 molecule remains bonded in the entire range of temperatures that was studied. Therefore the C_2 molecule can be considered as a single impurity with a large radius of interaction with Ni atoms.

This effect is in accordance with the behavior of bulk material where it is known that defects in crystalline lattice provide nucleation sites for the liquid state (see, e.g., Ref. 69 and references therein). For example, the melting point of the bulk iron carbide decreases to a minimum at a carbon concentration of 8.7%. Doping of large iron clusters (up to 2400 atoms) with 10% of carbon results in a reduction in the cluster melting point by approximately 10%.[29] However such an effect strongly depends on the type of impurity. As was demonstrated in Ref. 28, doping of the Ag_{55} cluster with Cu and Ni impurities in the center (where the bond length between Ag atoms and atoms of impurity are considerably smaller than the bond length between Ag atoms[28,69]) results in an increase in the melting temperature of the system. The elegant explanation of this effect has been conducted by Mottet *et al.* in Ref. 28. This explanation is closely related to the fundamental question of why small nickel clusters prefer icosahedral structures, while nickel clusters of an intermediate size (more than 1600 atoms) have decahedral structures, but bulk nickel and large nickel clusters of more than 10^5 atoms prefer a close-packed face-centered-cubic (fcc) structure.[88] The reason for such evolution in the cluster structure with increasing size is a competition between surface energies and elastic strain energies in the cluster. The latter arises due to distortion of the cluster lattice, where the intershell atomic distances are contracted in comparison with the intrashell distances.[28,88,89] The elastic strain energy of the icosahedral cluster is proportional to its volume. Therefore as the cluster size increases, the elastic strain energy increases as N, the number of atoms. On the other hand, the surface energy increases slower as it is proportional to the surface area, i.e., $N^{2/3}$. Hence, at some critical size the decahedral sequence of clusters becomes energetically more favorable than the icosahedral sequence because it is less strained, despite the larger surface energy. Similarly, because of the lack of strain in the fcc structures, the latter becomes lower in energy than the decahedra at larger sizes.[88,89] The doping of a cluster with an impurity near its center effectively allows one to manipulate the elastic strain energy—and with that, the cluster's stability and its melting temperature can also be tuned. It was demonstrated in Ref. 28 that a substitution of the central Ag atom with an atom of Cu or Ni induces the contraction of the cluster lattice in the vicinity of the cluster core, causing a partial release of the strain in the icosahedral structure.[28] Thus the small impurity in the center allows the cluster to relax toward a configuration with better interatomic distances, in other words, increasing the cluster stability.[28,69]

Our results demonstrate that doping of the C atom in the vicinity of the center of the Ni_{147} cluster induces an additional deformation in the cluster structure and, as a result, the melting temperature of the cluster decreases. To study in detail how this induced strain can change the thermodynamic behavior of the C-doped Ni_{147} cluster, we have performed calculations of the melting temperature of the cluster for the set of different parameters ρ and r_0 in Morse potential (3)—in other words, modeling the variation in the Ni-C interaction.

Curve 1 in Fig. 7 presents the dependence of the Morse potential $V^{\text{Ni-C}}(r)$ on the interatomic distance r calculated for the optimal values of the parameters ε_M, ρ, and r_0. Curve 2 in Fig. 7 presents the potential $V^{\text{Ni-C}}(r)$ when the bond constant r_0 and parameter ρ are reduced by the factor 0.5 in comparison to their optimal values, while curve 3 in Fig. 7 presents the interaction potential $V^{\text{Ni-C}}(r)$ when the parameters r_0 and ρ are enlarged by the factor 1.5. Hence, the potentials presented in Fig. 7 by curves 2 and 3 model the impurity effect with the local compression and expansion of the cluster lattice, respectively.

To illustrate the effect on the cluster structure due to the variation in the Ni-C interaction, we present in Figs. 8(a)–8(c) the histogram of the radial distribution of the number of Ni atoms located at distances between r and $r+\Delta r$ from the center of mass of the C-doped Ni_{147} cluster (where the width of the radial interval is Δr=0.001 Å). Location of the C impurity in the cluster is marked by an arrow. The change in the cluster structure, due to varying the parameters of ρ and r_0 in the Morse potential, can thus be clearly seen. For comparison, Fig. 8(d) represents the histogram of the

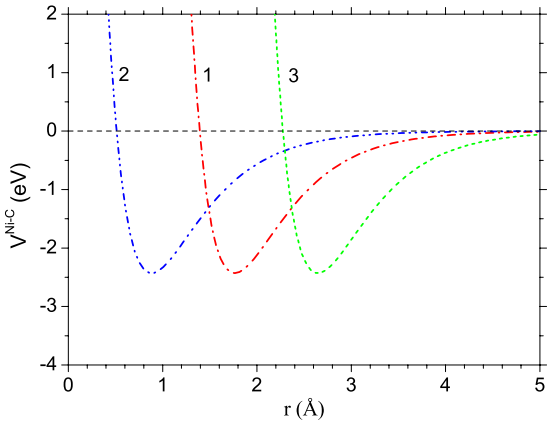

FIG. 7. (Color online) Morse potential for the Ni-C interaction with different values of parameters ρ and r_0. *Curve 1*: $\rho=3.295$, $r_0=1.763$ Å (optimal values); *curve 2*: $\rho=1.648$, $r_0=0.882$ Å (reduced bonding); and *curve 3*: $\rho=4.943$, $r_0=2.645$ Å (enlarged bonding). The depth of the potential well is kept constant, $\varepsilon_M=2.431$ eV.

radial distribution of the number of Ni atoms in the pure Ni_{147} cluster.

In the case of the reduced bonding between the C impurity and the Ni atoms, the overall icosahedral shell structure of the cluster remains preserved—although there exists some relaxation of the lattice [Fig. 8(a)]. The increase in the effective radius of the Morse potential for the Ni-C interaction results in strong distortions of the icosahedral shell structure of the cluster [Figs. 8(b) and 8(c)]. Such distortions reduce the stability of the cluster in comparison to the compact icosahedral structure. Additionally, one can see from Figs. 8(b) and 8(c) that the distortion occurs in the whole volume of the cluster. This is not surprising, as the cluster radius $R \approx 7.26$ Å is comparable with the radius of the Ni-C interaction. For large clusters, on the other hand, the local deformations that are induced by the impurity are not evenly distributed throughout the entire cluster. It is also worth mentioning that the location of the carbon impurity is sensitive to the range of the Ni-C interaction. In the all cases considered, the carbon impurity is located between the first and the second closed icosahedral shells. In the case of the short-range interaction, the impurity is located closer to the second icosahedral shell; however, increasing the interaction range causes the impurity atom to be pushed out toward the first shell. In general, the position of impurities in atomic clusters depends on many important factors not only for the case of a single impurity but also for alloy systems.[69] Whether the impurity atoms are mixed with or segregated from the host atoms is dependent on the relative strengths of (a) the bonds between

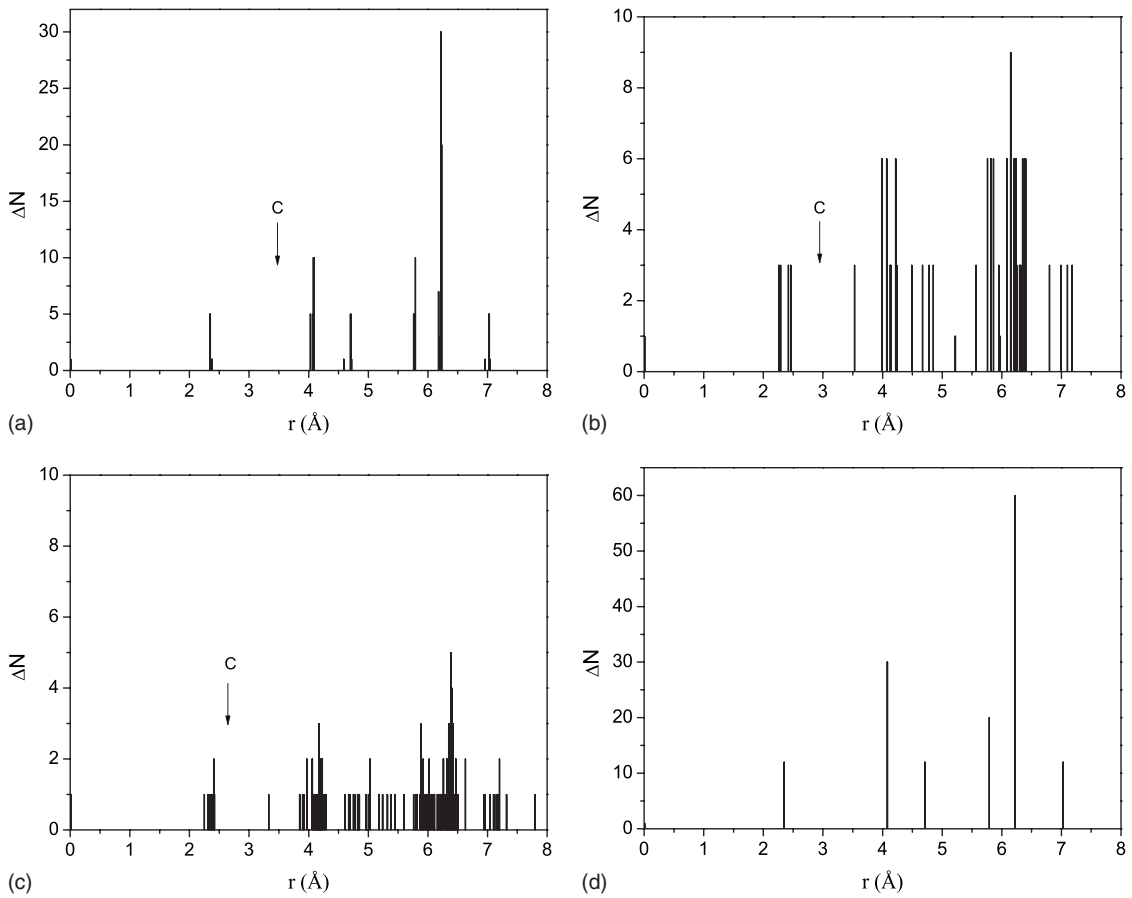

FIG. 8. The number of Ni atoms ΔN at distances between r and $r+\Delta r$ from the center of mass of the C-doped Ni_{147} cluster calculated for different values of the parameters ρ and r_0: (a) $\rho=1.648$, $r_0=0.882$ Å (reduced bonding); (b) $\rho=3.295$, $r_0=1.763$ Å (optimal values); (c) $\rho=4.943$, $r_0=2.645$ Å (enlarged bonding); and (d) pure Ni_{147} cluster for comparison. Location of the C impurity is marked by an arrow. The radial interval Δr is 0.001 Å.

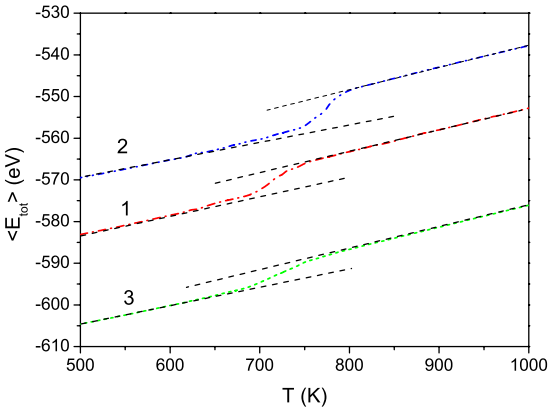

FIG. 9. (Color online) Caloric curves for the C-doped Ni_{147} cluster calculated for the different values of parameters ρ and r_0. Curve 1: ρ=3.295, r_0=1.763 Å (optimal values); curve 2: ρ =1.648, r_0=0.882 Å (reduced bonding); and curve 3: ρ=4.943, r_0=2.645 Å (enlarged bonding). The depth of the potential well is kept constant, ε_M=2.431 eV. (Dashed lines) Extrapolation of the frozen and molten branches of the caloric curve to estimate the latent heat. The total simulation time is 10 ns.

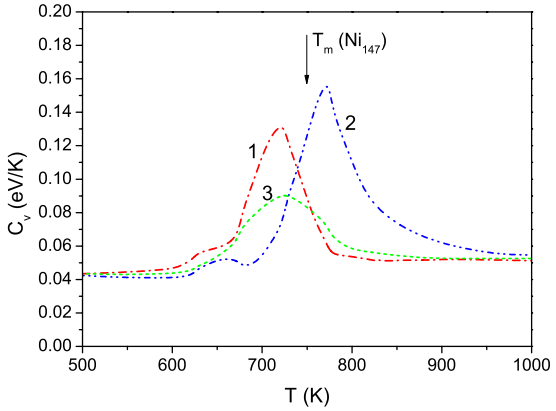

FIG. 10. (Color online) Heat capacity for the C-doped Ni_{147} cluster calculated for the different values of parameters ρ and r_0. Curve 1: ρ=3.295, r_0=1.763 Å (optimal values); curve 2: ρ =1.648, r_0=0.882 Å (reduced bonding); and curve 3: ρ=4.943, r_0=2.645 Å (enlarged bonding). The depth of the potential well is kept constant, ε_M=2.431 eV. Arrow indicates the melting temperature of the pure Ni_{147} cluster.

the host atoms of the cluster, (b) the bonds between the impurity (or alloy) atoms, or (c) the bond between the impurity atoms and the atoms of the host cluster.[69] Furthermore, the strongest bonds tend to be found at the cluster core, while elements with the lowest surface energy tend to be at the cluster surface. Smaller atoms tend to occupy the more stressed cluster core, especially in icosahedral clusters. In addition to the above factors, the size of the cluster, its compositions, and/or segregation arrangements can be stabilized by the electronic shell effects or the electron spin interaction, etc. Thus, the atomic arrangement of particular systems depends critically on the balance of these factors.[69]

Figures 9 and 10 demonstrate the temperature dependence of the caloric curve and the heat capacity of the C-doped Ni_{147} cluster calculated for different parameters of the Morse potential $V^{Ni\text{-}C}(r)$. Curve 1 in Figs. 9 and 10 presents the caloric curve and the heat capacity calculated with the optimal values of parameters for the Ni-C interaction.

Decreasing the effective radius of the Morse potential (see curve 2 of Fig. 7) by a factor 0.5 (cf. the optimal values) results in the contraction of the cluster lattice in the vicinity of the impurity. This contraction releases the strain in the icosahedral structure, thereby leading to an increase in the cluster stability. In this case, the melting temperature of the impurity doped Ni_{147} cluster increases by 21 K, as compared to the pure cluster (see curve 2 of Fig. 10). When the effective radius of the Morse potential for the Ni-C interaction is increased from its optimal value (see curve 1 in Fig. 7), the cluster lattice is further strained; thus the melting temperature of the C-doped Ni_{147} cluster decreases compared to the pure Ni_{147} cluster.

The process described above is quite similar to the process of the melting-point depression in partially oxidized sodium clusters.[27] It was demonstrated in Ref. 27 that the oxidized part of the solid sodium cluster shrinks, thus causing the metallic part to be under tension. The related deformation energy is accumulated in the metal. In contrast to the solid cluster, the liquid one follows the contraction of the oxidized core.[27] Therefore one can say that melting releases the stress of the oxidized sodium cluster, thereby thermodynamically promoting the liquid state. Hence, this is why the melting-point reduction is observed.[27] As was discussed in Ref. 27, the melting-point depression can also be interpreted as a surface effect, driven by the oxide-metal interface even though the whole cluster is involved. Due to the differences between the lattices of the pure metal and the oxide, the interfacial energy is larger when the whole cluster is solid, hence leading to the melting-point depression.[27]

A similar situation occurs in metal-carbide clusters. The metal-carbide core in a nickel cluster causes an additional strain in the cluster lattice. The accumulated energy can be interpreted as a surface energy in the interface between the impurity and the metal cluster. Hence, the related surface energy decreases upon melting, stabilizing the liquid phase and depressing the melting point.

The further increase in the effective radius of the Ni-C interaction creates a strong deformation and rearrangement in the cluster structure [see Fig. 8(c)], thereby lowering its melting temperature. Noticeably, the shift of the melting temperature and the overall temperature dependence of the heat capacity of the C-doped Ni_{147} cluster with the enlarged bonding parameters for the Ni-C interaction are rather similar to those for the C_2-doped Ni_{147} cluster. As was mentioned above, the C_2 molecule remains bonded within the entire range of temperatures considered. Hence, the C_2 can be considered as a single impurity with a large radius of interaction with the Ni atoms.

The change in the melting point upon doping can be a general phenomenon for nanoparticles with impurities. Depending on the type of interaction between the impurity and the atoms in the host cluster, the impurity causes a perturbation on the cluster lattice, leading to a stabilization or a destabilization of the system. This effectively causes a change in the melting temperature of the whole system. This is especially true when the size mismatch between atoms in the

cluster and impurity is large. Our calculations demonstrate that doping of the Ni_{147} cluster with C and C_2 impurities lowers its melting temperature by 30 K. A similar effect has been reported for Al, Ga, and Fe clusters doped with C impurities[26,30] and for Na clusters doped with Li, Cs, and O_2 impurities.[25,27] However, doping of Ag clusters with Ni and Cu impurities increases its melting temperature.[28] We suppose that doping of the host cluster with an impurity whose atomic size is smaller to that of the host atoms will lead to the penetration of the impurity to the cluster core, releasing the elastic stress, effectively stabilizing the system, and increasing its melting temperature. Such a situation has been described in Ref. 28. Another striking example can be found for Cu-Au clusters consisting of 55 atoms.[24] The lower energy structure of the Au_{55} cluster is not icosahedral; however by doping the Au_{55} cluster with a single Cu impurity in the cluster center stabilizes the icosahedral structure of $Au_{54}Cu_1$.[24] The opposite case occurs when a larger-sized impurity (compared to the host atoms) deforms the cluster lattice; this causes destabilization of the cluster structure and leads to the lowering of the melting temperature.

Figure 10 demonstrates that the height of the heat capacity peak decreases with an increase in the range of the Ni-C interaction. Note that the influence of the potential range on the heat capacity of the 13-atom Morse clusters has been studied in Ref. 90. It was found that decreasing the range of the potential increases the peak of the heat capacity in the melting transition region. A similar effect has been observed in the series Na→K→Rb→Cs.[84] It is interesting that a similar behavior is also seen for the doped clusters: increasing the radius of interaction between Ni atoms and single C impurity considerably lowers the peak of the heat capacity.

It is also seen from Fig. 10 that the premelting effect diminishes with an increase in the effective radius of the Ni-C interaction and so cannot be distinguished from the model case of an enlarged bonding between the impurity and the Ni atoms (curve 3 in Fig. 7). As we have already mentioned, the increase in the effective radius of the Ni-C interaction creates a strong volume and surface rearrangement of the cluster structure, thus lowering its symmetry. Hence, a smooth melting transition is observed with an increase in the number of nonequivalent atoms on the surface of the cluster.

As it was shown in Ref. 13, the complex size-dependent fluctuations of the melting temperature of sodium clusters can be understood in terms of the energy and entropy differences between the molten and the frozen states of the cluster. For the canonical ensemble the melting temperature can be defined as a ratio of the latent heat, ΔE, and the change of entropy, ΔS, at the melting point,

$$T_m = \frac{\Delta E}{\Delta S}. \tag{5}$$

Table I summarizes the values for the melting temperature, latent heat, and change in entropy calculated for the pure and C-doped Ni_{147} clusters at the point of phase transition. Here the melting temperature, T_m corresponds to the maximum of the heat capacity, latent heat, and ΔE, defined from the corresponding caloric curves at the point of phase transition, and the entropy change, ΔS, is calculated with the use of relation (5). As it is seen from Table I, the change in the melting temperature of the Ni_{147} cluster due to C doping is stipulated by the interplay of contributions from the latent heat and the entropy change upon melting.

TABLE I. Melting temperature, T_m, latent heat, ΔE, and entropy change, ΔS, calculated for the pure and C-doped Ni_{147} clusters at the point of phase transition.

	T_m (K)	ΔE (eV)	ΔS (k_B)
Ni_{147}	750	7.5 ± 0.2	116 ± 3
C-doped Ni_{147} (optimal bonding)	720	6.0	96
C-doped Ni_{147} (reduced bonding)	771	8.0	120
C-doped Ni_{147} (enlarged bonding)	725	4.2	67
C_2-doped Ni_{147}	725	6.2	99

When the effective radius of the Ni-C interaction is decreased from its optimal values (see curve 2 of Fig. 7), the cluster core becomes firmly linked. Hence, the latent heat is larger than that for the pure Ni_{147} cluster. The symmetry of the system remains mostly untouched, resulting in a small variation in the entropy change in comparison with the Ni_{147} cluster. For these reasons, the melting temperature of the C-doped Ni_{147} cluster becomes larger than that for the pure Ni_{147} cluster.

Conversely, when the effective radius of the Ni-C interaction is increased or at its optimal value, both the latent heat and entropy change in the C-doped Ni_{147} cluster decrease considerably compared to the pure Ni_{147} cluster, leading to a decrease in the melting temperature of the C-doped Ni_{147} cluster (see Table I). However, while the optimal C-doped Ni_{147} cluster is more disordered, the melting temperature of the C-doped Ni_{147} cluster with the increased effective radius is just slightly larger than that of the C-doped Ni_{147} cluster with the optimal effective radius.

The melting transition can also be recognized from the analysis of the trajectories of the individual atoms and their diffusion in the volume of the cluster. The melting transition occurs when atoms begin their Brownian motion instead of the thermal vibrations about their equilibrium positions in the ordered cluster's lattice. Such a transition can be seen as a step in the temperature dependence of the diffusion coefficient. The diffusion coefficient of the atom i in a media is defined as (see, e.g., Refs. 86 and 91)

$$D_i = \frac{1}{6}\frac{d}{dt}\langle r_i^2(t)\rangle, \tag{6}$$

where $\langle r_i^2(t)\rangle$ is the mean-square displacement averaged along the atom's trajectory,

$$\langle r_i^2(t)\rangle = \frac{1}{n_t}\sum_{j=1}^{n_t}[\mathbf{R}_i(t_{0j}+t) - \mathbf{R}_i(t_{0j})]^2. \tag{7}$$

Here $\mathbf{R}_i(t)$ is a radius vector of an atom i at the time t and n_t is the number of time origins, t_{0j}, considered along the trajectory. Equation (6) is valid for the simulation time smaller

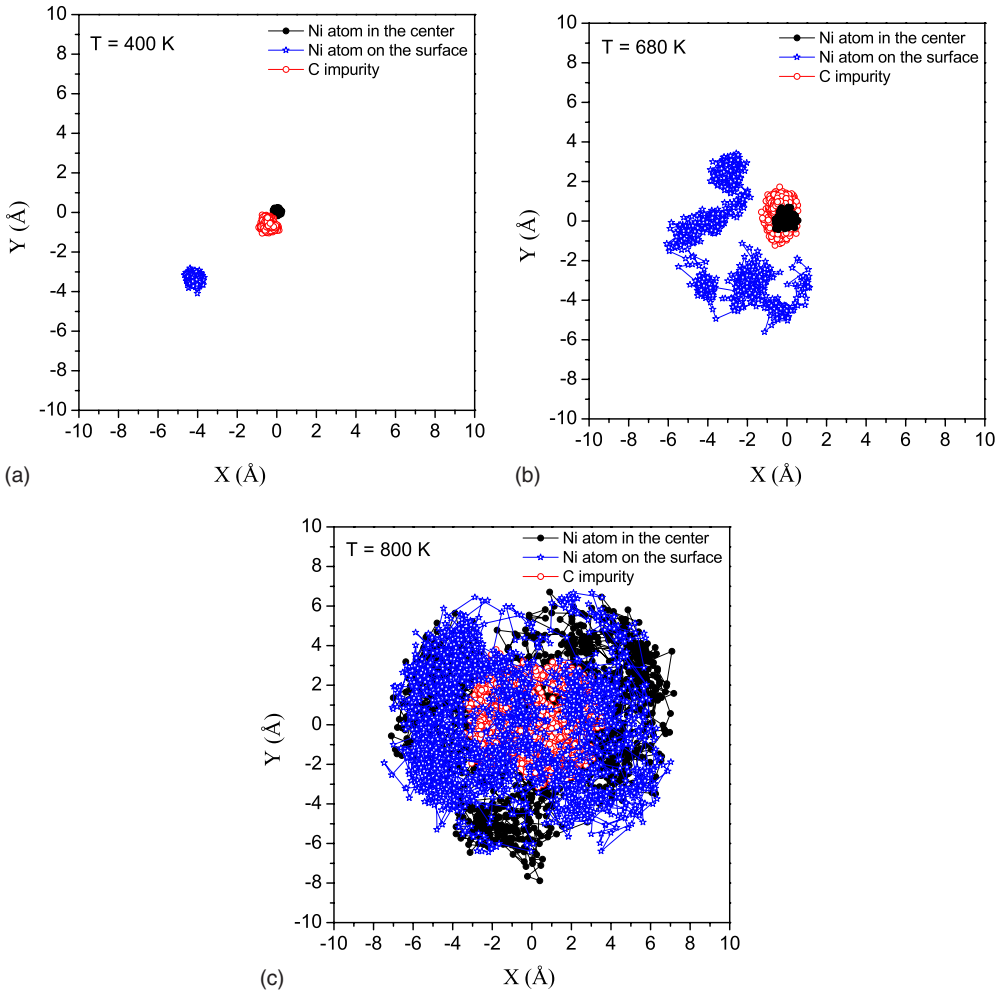

FIG. 11. (Color online) The 2D projection of trajectories calculated for the Ni atom in the center of the C-doped Ni_{147} cluster (filled dots), the Ni atom from the vertex of the cluster surface (stars), and the C impurity (open dots) for the cluster temperatures T=400, 680, and 800 K. The output time step is 1 ps and the total simulation time is 2 ns.

than the time required for a particle to migrate across the diameter of the cluster.

Figure 11 demonstrates the two-dimensional (2D) projection of trajectories calculated for the Ni atom in the center of the C-doped Ni_{147} cluster (filled dots), the Ni atom from the vertex of the cluster surface (stars), and the C impurity (open dots). The temperature of the cluster ranges from 400 to 800 K, as is shown in Fig. 11. The output time step is 1 ps with the total simulation time of 2 ns.

As seen in Fig. 11, for a low temperature, T=400 K, all selected atoms in the C-doped Ni_{147} cluster vibrate about their equilibrium positions. At this temperature, the cluster is frozen—as per the analysis of the caloric curve and the heat capacity calculated for the C-doped Ni_{147} cluster (see Figs. 5 and 6).

It has been discussed above that the temperature dependence of the heat capacity of the C-doped Ni_{147} cluster exhibits two maxima corresponding to surface and volume melting of the cluster. It is seen from Fig. 6 that the first maximum in the temperature dependence of the heat capacity appears when the cluster is at T=640 K (surface melting), while the second maximum appears at T=720 K (volume melting). The temperature of 680 K corresponds to the intermediate state when the surface of the cluster has already melted but the cluster core is still frozen, as confirmed by the analysis of the atomic trajectories. As can be seen in Fig. 11 at T=680 K, the surface Ni atom begins to diffuse on the surface, while the central Ni atom and the C impurity are still vibrating about their equilibrium positions. Note that the icosahedral surface is inhomogeneous and consists of 12 vertices, 20 faces, and 30 edges. The binding energies of the atoms taken from the vertices, faces, and edges are thus slightly different. Hence, these atoms begin diffusion at different temperatures.

Finally at the temperature of 800 K, cluster has completely melted as can be observed from the temperature behavior of the heat capacity presented in Fig. 6. Figure 11 demonstrates that the Ni atoms are moving in the entire volume of the cluster. The C impurity is also moving randomly in the cluster volume although the movement only occurs in the central part of the cluster. Hence, this supposes the heterogeneous distribution of the C atoms in the melted Ni_{147} clusters at T=800 K.

The change in cluster structure upon melting is clearly seen in the time-averaged radial distribution of atoms in the

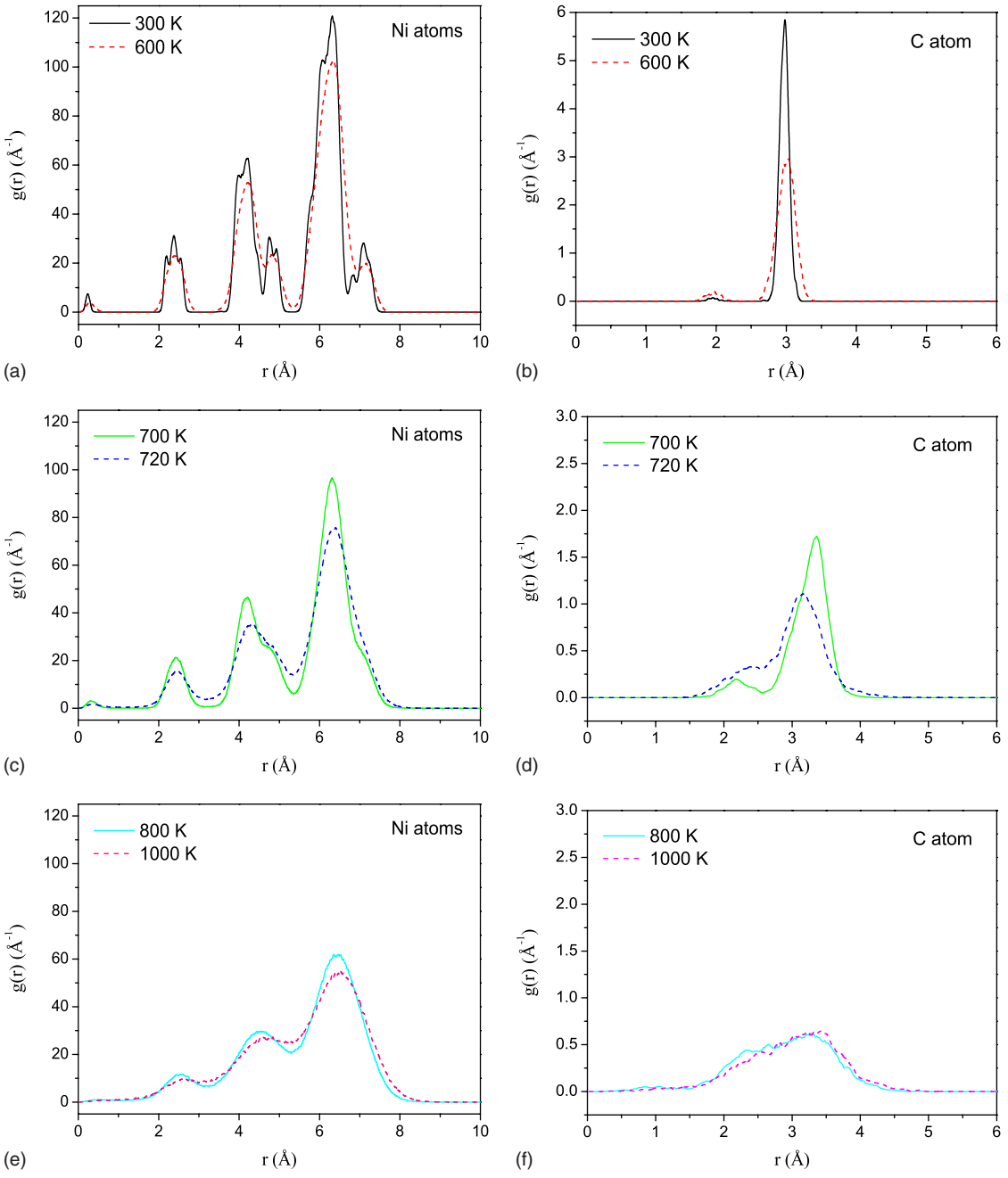

FIG. 12. (Color online) The time-averaged radial distribution function $g(r)$ calculated for the Ni and C atoms in the C-doped Ni_{147} cluster at different temperatures. The total simulation time is 10 ns.

cluster. The radial atomic distribution function $g(r)$ is defined as

$$g(r) = dN(r)/dr, \tag{8}$$

where $dN(r)$ is the number of atoms in the spherical layer at distances between r and $r+dr$ from the center of mass of the cluster.

Figure 12 demonstrates the time-averaged radial distribution function $g(r)$ for Ni and C atoms in the C-doped Ni_{147} cluster calculated at cluster temperatures of $T=300$, 600, 700, 720, 800, and 1000 K. The chosen range of temperatures allows for the analysis of the cluster structure in the frozen, transitional, and molten states.

At the low cluster temperature, $T=300$ K, one can see the icosahedral shell structure of the nickel subsystem of the C-doped Ni_{147} cluster, consisting of the central atom and three icosahedral shells. The second and third shells are split—corresponding to atoms in vertex (12 atoms per shell) and nonvertex positions. Heating the cluster up to 600 K washes out the subshell splitting; nonetheless the icosahedral shells remain well separated.

With increase in the cluster temperature, up to 700 K, the second and the third shells begin to merge, although the first and the second shells are still separated [i.e., the radial dis-

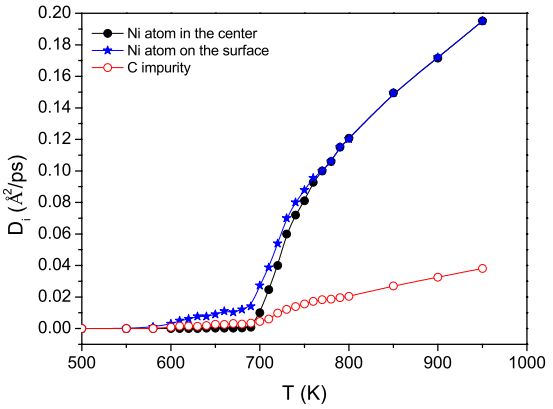

FIG. 13. (Color online) Temperature dependence of diffusion coefficients calculated for the Ni atom in the center of the C-doped Ni_{147} cluster (filled dots), the Ni atom on the cluster surface (stars), and the C impurity (open dots).

tribution function $g(r)$ is equal to zero in the space between shells]. At the temperature corresponding to the maximum in the heat capacity of the C-doped Ni_{147} cluster, $T=720$ K, the first and second icosahedral shells merge.

Finally, at the temperatures corresponding to the molten state (800 and 1000 K in Fig. 12), the distribution of Ni atoms becomes more homogeneous and the sharp shell structure washes out. Nevertheless, even at $T=1000$ K, some radial order with maxima at 2.6, 4.6, and 6.5 Å still remains, suggesting that even a molten cluster of a finite size manifests some signs of a shell structure. This effect might be a general feature of finite systems, similar to the surface-induced ordering in liquid crystals or the layering effect at free liquid surfaces.[25,92,93]

Figure 12 demonstrates that, at cluster temperatures of 300 and 600 K, the time-averaged radial distribution function calculated for the C impurity atom exhibits a sharp maximum at distances of 3 Å from the center of mass of the C-doped Ni_{147} cluster. Thus, at these temperatures, the C impurity is located between the first and the second icosahedral shells of the Ni atoms. By further increasing the cluster temperature to temperatures near the phase transition region, the radial distribution $g(r)$ of the C impurity becomes wider and the appearance of a second maximum at distances ≈ 2 Å can be observed. While at $T>800$ K, the C impurity can be found to be distributed in the central part of the cluster.

Figure 13 demonstrates the temperature dependence of diffusion coefficients calculated for the selected atoms in the C-doped Ni_{147} cluster. It is seen from Fig. 13 that the Ni atom on the cluster surface begins to diffuse at temperature of 600 K, while the Ni atom in the cluster center and the C impurity remain frozen.

As has been shown above, the caloric curve calculated for the C-doped Ni_{147} cluster (see Fig. 5) clearly demonstrates a stepwise melting behavior. In the temperature interval $600\ \text{K}<T<700$ K, the slope of the caloric curve changes slightly in comparison with that for the frozen state, suggesting the existence of a premelted state. For temperatures $700\ \text{K}<T<760$ K, the time-averaged total energy $\langle E_{\text{tot}}\rangle$ grows rapidly and finally reaches its asymptotic behavior at $T>760$ K. The variations in the slope of the caloric curve result in the appearance of the two maxima in the temperature-dependent heat capacity. These maxima are associated with the surface and core (volume) melting of the C-doped Ni_{147} cluster. This proposition is fully confirmed by the analysis of the temperature dependence of the diffusion coefficients for the Ni atoms from (a) the cluster surface and (b) the cluster center.

Thus, in the temperature interval of $600\ \text{K}<T<700$ K, only surface atoms diffuse, confirming the initial melting of the cluster surface. The Ni atom located in the cluster center then begins to diffuse at $T=700$ K. The diffusion coefficients calculated for the Ni atoms located on the cluster surface and in the core are different up to $T=760$ K. The difference in the diffusion coefficients shows that the surface and the core atoms are not yet fully mixed in the cluster volume. This difference disappears when $T>760$ K, corresponding to the completely molten state of the C-doped Ni_{147} cluster.

Figure 13 demonstrates that the C impurity begins to diffuse at $T\approx 700$ K—similar to the central Ni atom. However, values of the diffusion coefficients calculated for the C impurity are considerably lower than those for the Ni atoms. Knowledge of the diffusion coefficients of the C impurity in a nickel cluster can be used for building a reliable kinetic model of carbon nanotube growth.[34,41]

IV. CONCLUSION

Doping of Ni_{147} with a carbon impurity lowers its melting temperature by 30 K due to excessive stress on the cluster lattice. The distortion of the cluster lattice results in the change in the cluster's energetics as well as its entropy. The magnitude of the change induced is dependent on the parameters of the interaction between the nickel atoms and the carbon impurity. We have demonstrated that an induced contraction of the icosahedral cluster's lattice in the vicinity of the impurity results in an increase in the melting temperature of the cluster, whereas additional strain in the lattice results in the reduction in the melting temperature. Therefore, the melting temperature of atomic clusters can be effectively tuned by the addition of an impurity of a particular type.

Doping by a C or C_2 impurity changes the melting temperature of the cluster; consequently this means that doping affects the mobility of the atoms in the Ni cluster. This effect has to be taken into consideration in particular applications with metal clusters when the entire process depends on the thermodynamic state of the cluster. An example of such experiment is the process of the catalytically activated growth of carbon nanotubes. The kinetics of the carbon nanotube growth depends on diffusion of carbon atoms through the metal catalyst. Presence of the impurities can considerably change the flux, thereby affecting the growth rate of the carbon nanotube. The additional change in the thermodynamic state of the catalytic particle in the nanotube growth process might also depend on the strength of the interaction of the particle with a substrate.

In the present work, we have considered a single C and C_2 impurity in the cluster of Ni_{147}. It is interesting to study how several C impurities will influence the thermodynamic prop-

erties of the host cluster. In particular, it is important to find the optimum conditions (concentration of C atoms, temperature, thermodynamic state of the particle, etc.) when the C atoms begin aggregating into ordered carbon structures, such as nanotubes. Such a study will require careful investigation of a reliable many-body potential for the C-C interactions in the host metal cluster.

The influence of impurities on properties of finite systems is a general effect. While our results were obtained for free clusters, many interesting problems can be found when one considers the influence of impurities on the phase transitions and stability of clusters deposited on a substrate. Thus, recently it has been experimentally shown that the oxidation of silver clusters deposited on a highly oriented pyrolytic graphite (HOPG) surface changes the stability and morphology of cluster formations.[94,95] Clusters on substrates have important technological applications and the understanding of how these clusters stabilize on the surface is of profound interest.

ACKNOWLEDGMENTS

This work was partially supported by the European Commission within the PECU project [Contract No. 4916 (NEST)] and Network of Excellence project EXCELL. The authors gratefully acknowledge support by the Frankfurt Center for Scientific Computing.

*On leave from Institute of Physics, St. Petersburg State University, Ulianovskaya Str. 1, 198504 St. Petersburg, Petrodvorez, Russia; lyalin@fias.uni-frankfurt.de

†On leave from A. F. Ioffe Physical-Technical Institute, Polytechnicheskaya 26, 194021 St. Petersburg, Russia.

[1] W. Thomson, Philos. Mag. **42**, 448 (1871).
[2] P. Pawlow, Z. Phys. Chem., Stoechiom. Verwandtschaftsl. **65**, 545 (1909).
[3] M. Takagi, J. Phys. Soc. Jpn. **9**, 361 (1954).
[4] K. J. Hanszen, Z. Phys. Chem. **157**, 523 (1960).
[5] Y. Qi, T. Çhağin, W. L. Johnson, and W. A. Goddard III, J. Chem. Phys. **115**, 385 (2001).
[6] Ph. Buffat and J.-P. Borel, Phys. Rev. A **13**, 2287 (1976).
[7] T. Castro, R. Reifenberger, E. Choi, and R. P. Andres, Phys. Rev. B **42**, 8548 (1990).
[8] S. L. Lai, J. Y. Guo, V. Petrova, G. Ramanath, and L. H. Allen, Phys. Rev. Lett. **77**, 99 (1996).
[9] C. E. Bottani, A. Li Bassi, B. K. Tanner, A. Stella, P. Tognini, P. Cheyssac, and R. Kofman, Phys. Rev. B **59**, R15601 (1999).
[10] M. Schmidt, R. Kusche, W. Kronmüller, B. von Issendorff, and H. Haberland, Phys. Rev. Lett. **79**, 99 (1997).
[11] M. Schmidt, R. Kusche, B. von Issendorff, and H. Haberland, Nature (London) **393**, 238 (1998).
[12] R. Kusche, Th. Hippler, M. Schmidt, B. von Issendorff, and H. Haberland, Eur. Phys. J. D **9**, 1 (1999).
[13] H. Haberland, Th. Hippler, J. Donges, O. Kostko, M. Schmidt, and B. von Issendorff, Phys. Rev. Lett. **94**, 035701 (2005).
[14] F. Calvo and F. Spiegelmann, J. Chem. Phys. **112**, 2888 (2000).
[15] J. A. Reyes-Nava, I. L. Garzon, and K. Michaelian, Phys. Rev. B **67**, 165401 (2003).
[16] F. Calvo and F. Spiegelmann, J. Chem. Phys. **120**, 9684 (2004).
[17] K. Manninen, A. Rytkonen, and M. Manninen, Eur. Phys. J. D **29**, 39 (2004).
[18] S. Chacko, D. G. Kanhere, and S. A. Blundell, Phys. Rev. B **71**, 155407 (2005).
[19] A. Aguado and J. M. López, Phys. Rev. Lett. **94**, 233401 (2005).
[20] A. Aguado, J. Phys. Chem. B **109**, 13043 (2005).
[21] E. G. Noya, J. P. K. Doye, D. J. Wales, and A. Aguado, Eur. Phys. J. D **43**, 57 (2007).
[22] A. A. Shvartsburg and M. F. Jarrold, Phys. Rev. Lett. **85**, 2530 (2000).
[23] G. A. Breaux, R. C. Benirschke, T. Sugai, B. S. Kinnear, and M. F. Jarrold, Phys. Rev. Lett. **91**, 215508 (2003).
[24] S. Darby, T. V. Mortimer-Jones, R. L. Johnston, and C. J. Roberts, J. Chem. Phys. **116**, 1536 (2002).
[25] A. Aguado, L. E. González, and J. M. López, J. Phys. Chem. B **108**, 11722 (2004).
[26] P. Chandrachud, K. Joshi, and D. G. Kanhere, Phys. Rev. B **76**, 235423 (2007).
[27] C. Hock, S. Straßburg, H. Haberland, B. v. Issendorff, A. Aguado, and M. Schmidt, Phys. Rev. Lett. **101**, 023401 (2008).
[28] C. Mottet, G. Rossi, F. Baletto, and R. Ferrando, Phys. Rev. Lett. **95**, 035501 (2005).
[29] F. Ding, K. Bolton, and A. Rosén, J. Vac. Sci. Technol. A **22**, 1471 (2004).
[30] A. Jiang, N. Awasthi, A. N. Kolmogorov, W. Setyawan, A. Börjesson, K. Bolton, A. R. Harutyunyan, and S. Curtarolo, Phys. Rev. B **75**, 205426 (2007).
[31] *Handbook of Nanoscience, Engineering, and Technology*, edited by W. A. Goddard III, D. W. Brenner, S. Lyshevski, and G. Iafrate (CRC, Cleveland, 2007).
[32] V. B. Golovko, H. W. Li, B. Kleinsorge, S. Hofmann, J. Geng, M. Cantoro, Z. Yang, D. A. Jefferson, B. F. G. Johnson, W. T. S. Huck, and J. Robertson, Nanotechnology **16**, 1636 (2005).
[33] O. I. Obolensky, I. A. Solov'yov, A. V. Solov'yov, and W. Greiner, *Book of Abstracts*, Symposium on Size Selected Clusters (S3C), Brand, Austria, 2007, p. 132.
[34] O. I. Obolensky, I. A. Solov'yov, A. V. Solov'yov, and W. Greiner, in *Abstracts of the International Symposium "Atomic Cluster Collisions: Structure and Dynamics from the Nuclear to the Biological Scale" (ISACC 2007)*, edited by A. V. Solov'yov (European Physical Society, Frankfurt am Main, 2007) [Europhys. Conf. Abstr. **31D**, 176 (2007)].
[35] T. Nozaki, Y. Kimura, and K. Okazaki, J. Phys. D **35**, 2779 (2002).
[36] J. Gavillet, A. Loiseau, C. Journet, F. Willaime, F. Ducastelle, and J.-C. Charlier, Phys. Rev. Lett. **87**, 275504 (2001).
[37] G. Y. Zhang, X. C. Ma, D. Y. Zhong, and E. G. Wanga, J. Appl. Phys. **91**, 9324 (2002).
[38] A. R. Harutyunyan, N. Awasthi, A. Jiang, W. Setyawan, E. Mora, T. Tokune, K. Bolton, and S. Curtarolo, Phys. Rev. Lett. **100**, 195502 (2008).

[39] S. Curtarolo, N. Awasthi, W. Setyawan, A. Jiang, K. Bolton, T. Tokune, and A. R. Harutyunyan, Phys. Rev. B **78**, 054105 (2008).
[40] A. R. Harutyunyan, T. Tokune, and E. Mora, Appl. Phys. Lett. **87**, 051919 (2005).
[41] O. A. Louchev, Th. Laude, Y. Sato, and H. Kanda, J. Chem. Phys. **118**, 7622 (2003).
[42] R. T. K. Baker and P. S. Harris, in *Chemistry and Physics of Carbon*, edited by P. L. Walker, Jr. and P. A. Thrower (Dekker, New York, 1978).
[43] S. Nayak, S. N. Khanna, B. K. Rao, and P. Jena, J. Phys. Chem. A **101**, 1072 (1997).
[44] A. P. Sutton and J. Chen, Philos. Mag. Lett. **61**, 139 (1990).
[45] M. S. Daw and M. I. Baskes, Phys. Rev. Lett. **50**, 1285 (1983).
[46] M. S. Daw and M. I. Baskes, Phys. Rev. B **29**, 6443 (1984).
[47] S. M. Foiles, M. I. Baskes, and M. S. Daw, Phys. Rev. B **33**, 7983 (1986).
[48] M. W. Finnis and J. E. Sinclair, Philos. Mag. A **50**, 45 (1984).
[49] A. P. Sutton, P. D. Godwin, and A. P. Horsfield, MRS Bull. **21**, 42 (1996).
[50] H. Rafii-Tabar and A. P. Sutton, Philos. Mag. Lett. **63**, 217 (1991).
[51] B. D. Todd and R. M. Lynden-Bell, Surf. Sci. **281**, 191 (1993).
[52] R. M. Lynden-Bell, J. Phys.: Condens. Matter **7**, 4603 (1995).
[53] J. P. K. Doye and D. Wales, New J. Chem. **22**, 733 (1998).
[54] Y. Yamaguchi and S. Maruyama, Eur. Phys. J. D **9**, 385 (1999).
[55] Y. Shibuta and S. Maruyama, Comput. Mater. Sci. **39**, 842 (2007).
[56] A. Martinez-Limia, J. Zhao, and P. Balbuena, J. Mol. Model. **13**, 595 (2007).
[57] C. Lee, W. Yang, and R. G. Parr, Phys. Rev. B **37**, 785 (1988).
[58] A. D. Becke, Phys. Rev. A **38**, 3098 (1988).
[59] A. D. Becke, J. Chem. Phys. **98**, 5648 (1993).
[60] James B. Foresman and Æleen Frisch, *Exploring Chemistry with Electronic Structure Methods* (Gaussian, Pittsburgh, PA, 1996).
[61] J. Tersoff, Phys. Rev. Lett. **61**, 2879 (1988).
[62] C. Rey, M. M. G. Alemany, O. Diéguez, and L. J. Gallego, Phys. Rev. B **62**, 12640 (2000).
[63] G. E. Froudakis, M. Mühlhäuser, A. N. Andriotis, and M. Menon, Phys. Rev. B **64**, 241401(R) (2001).
[64] I. A. Solov'yov, A. V. Solov'yov, W. Greiner, A. Koshelev, and A. Shutovich, Phys. Rev. Lett. **90**, 053401 (2003).
[65] I. A. Solov'yov, A. V. Solov'yov, and W. Greiner, Int. J. Mod. Phys. E **13**, 697 (2004).
[66] O. I. Obolensky, I. A. Solov'yov, A. V. Solov'yov, and W. Greiner, Comput. Let. **1**, 313 (2005).
[67] D. E. Goldberg, *Genetic Algorithms in Search, Optimization, and Machine Learning* (Addison-Wesley, Reading, MA, 1989).
[68] Z. Michalewicz, *Genetic Algorithms + Data Structures = Evolution Programs*, 3rd ed. (Springer, Berlin, 1996).
[69] R. Ferrando, J. Jellinek, and R. L. Johnston, Chem. Rev. (Washington, D.C.) **108**, 845 (2008).
[70] A. Lyalin, I. A. Solov'yov, A. V. Solov'yov, and W. Greiner, Phys. Rev. A **67**, 063203 (2003).
[71] A. Lyalin, A. V. Solov'yov, and W. Greiner, Phys. Rev. A **74**, 043201 (2006).
[72] A. Lyalin, I. A. Solov'yov, A. V. Solov'yov, and W. Greiner, Phys. Rev. A **75**, 053201 (2007).
[73] S. Nose, J. Chem. Phys. **81**, 511 (1984).
[74] W. G. Hoover, Phys. Rev. A **31**, 1695 (1985).
[75] J. A. Alonso, *Structure and Properties of Atomic Nanoclusters* (Imperial, London, 2005).
[76] F. Baletto and R. Ferrando, Rev. Mod. Phys. **77**, 371 (2005).
[77] M. Pellarin, B. Baguenard, J. L. Vialle, J. Lermé, M. Broyer, J. Miller, and A. Perez, Chem. Phys. Lett. **217**, 349 (1994).
[78] J. M. Montejano-Carrizales, M. P. Iñiguez, J. A. Alonso, and M. J. López, Phys. Rev. B **54**, 5961 (1996).
[79] Z. Zhang, W. Hua, and S. Xiao, J. Chem. Phys. **122**, 214501 (2005).
[80] *Chemistry and Physics of Solid Surfaces VII*, edited by R. Canselow and R. F. Howe (Springer, Heidelberg, 1988).
[81] C. Kittel, *Introduction to Solid State Physics*, 7th ed. (Wiley, New York, 1996).
[82] C. Rey, J. García-Rodeja, L. J. Gallego, and M. J. Grimson, Phys. Rev. E **57**, 4420 (1998).
[83] A. Aguado, J. M. López, J. A. Alonso, and M. J. Stott, J. Chem. Phys. **111**, 6026 (1999).
[84] A. Aguado, Phys. Rev. B **63**, 115404 (2001).
[85] A. Aguado and J. M. López, Phys. Rev. B **74**, 115403 (2006).
[86] J. Jellinek, T. L. Beck, and R. S. Berry, J. Chem. Phys. **84**, 2783 (1986).
[87] H. L. Davis, J. Jellinek, and R. S. Berry, J. Chem. Phys. **86**, 6456 (1987).
[88] C. L. Cleveland and U. Landman, J. Chem. Phys. **94**, 7376 (1991).
[89] J. P. K. Doye, D. Wales, and R. S. Berry, J. Chem. Phys. **103**, 4234 (1995).
[90] M. Moseler and J. Nordiek, Phys. Rev. B **60**, 11734 (1999).
[91] L. D. Landau and E. M. Lifshitz, *Fluid Mechanics*, Course of Theoretical Physics Vol. 6, 2nd ed. (Pergamon, New York, 1987).
[92] B. M. Ocko, A. Braslau, P. S. Pershan, J. Als-Nielsen, and M. Deutsch, Phys. Rev. Lett. **57**, 94 (1986).
[93] E. Chacón, M. Reinaldo-Falagán, E. Velasco, and P. Tarazona, Phys. Rev. Lett. **87**, 166101 (2001).
[94] A. Lando, N. Kébaïli, Ph. Cahuzac, A. Masson, and C. Bréchignac, Phys. Rev. Lett. **97**, 133402 (2006).
[95] A. Lando, N. Kébaïli, Ph. Cahuzac, C. Colliex, M. Couillard, A. Masson, M. Schmidt, and C. Bréchignac, Eur. Phys. J. D **43**, 151 (2007).